ACSNANO
www.acsnano.org
ARTICLE

Characteristic Contrast in Δf_{min} Maps of Organic Molecules Using Atomic Force Microscopy

Nadine J. van der Heijden,[†] Prokop Hapala,[‡] Jeroen A. Rombouts,[§] Joost van der Lit,[†] Daniël Smith,[†] Pingo Mutombo,[‡] Martin Švec,[‡] Pavel Jelinek,[‡] and Ingmar Swart*[,†]

[†]Condensed Matter and Interfaces, Debye Institute for Nanomaterials Science, Utrecht University, P.O. Box 80000, 3508 TA Utrecht, The Netherlands

[‡]Institute of Physics, Czech Academy of Sciences, Cukrovarnická 10, 1862 53 Prague, Czech Republic

[§]Department of Chemistry and Pharmaceutical Sciences, VU University Amsterdam, De Boelelaan 1083, 1081 HV Amsterdam, The Netherlands

Supporting Information

ABSTRACT: **Scanning tunneling microscopy and atomic force microscopy can provide detailed information about the geometric and electronic structure of molecules with submolecular spatial resolution. However, an essential capability to realize the full potential of these techniques for chemical applications is missing from the scanning probe toolbox: chemical recognition of organic molecules. Here, we show that maps of the minima of frequency shift−distance curves extracted from 3D data cubes contain characteristic contrast. A detailed theoretical analysis based on density functional theory and molecular mechanics shows that these features are characteristic for the investigated species. Structurally similar but chemically distinct molecules yield significantly different features. We find that the van der Waals and Pauli interaction, together with the specific adsorption geometry of a given molecule on the surface, accounts for the observed contrast.**

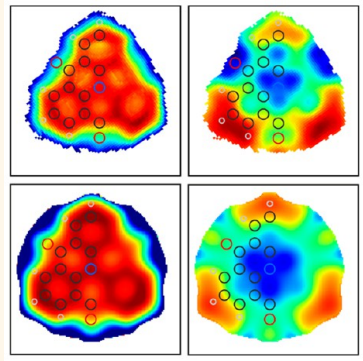

KEYWORDS: *AFM, DFT, molecular mechanics, single molecule, CO tip, Xe tip*

Scanning tunneling microscopy (STM) and atomic force microscopy (AFM) are both capable of imaging molecules with submolecular resolution.[1−5] In addition, both techniques can provide quantitative information: STM on the electronic structure and AFM on the charge distribution and the bond orders.[5−8] Hence, both techniques find increasing use in the field of chemistry. To realize the full potential of STM and AFM in studies involving molecules, the ability to identify or recognize molecules is of great value. STM provides chemical recognition capabilities *via* inelastic electron tunneling spectroscopy *via* differences in the local density of states and vibration frequencies of bonds.[9−12] Force−distance spectroscopy, combined with density functional theory (DFT) calculations, has been used to chemically identify atoms in surfaces of insulators, alloys, and semiconductors.[13−19] In most cases, the origin of the chemical contrast is due to formation of atom-specific covalent bonds with the tip. However, submolecular resolution imaging of molecules requires the use of chemically passivated tips to avoid an accidental pickup of the molecule of interest. Hence, chemical recognition of atoms within an organic molecule has to rely on a different contrast mechanism. Contrast differences in AFM images over various chemical elements in organic molecules have been observed, indicating that elemental identification may be possible.[20−22] Thus far, chemical recognition with AFM has mostly relied on structural arguments.[20−22]

The chemical identification procedure for atoms in an alloy surface[14] cannot be transferred to recognize organic molecules adsorbed on a surface. First, the chemical contrast observed on surfaces is due to the formation of a (partial) covalent bond between the reactive metal tip and the atoms under investigation. This is in direct conflict with the requirement to use chemically passivated tips. Another complication that hampers direct chemical identification of atoms in molecules by comparing frequency shift−distance ($\Delta f(z)$) spectra is the fact that the van der Waals (vdW) force varies strongly over a single molecule on a surface.[23] Hence, $\Delta f(z)$ spectra acquired over identical elements in a molecule, one at the center and the other at the periphery, will be significantly different. This is especially important because for most organic molecules the majority of the atoms reside at the periphery. However, it is important to realize that chemical recognition of molecules does *not* require each atom in a molecule to be identified separately. Instead, it is sufficient if the molecule as a whole exhibits some characteristic contrast. Since the overall magnitude and shape of the potential energy landscape experienced by the tip should reflect both the geometry

Received: June 2, 2016
Accepted: August 10, 2016
Published: August 10, 2016

DOI: 10.1021/acsnano.6b03644
ACS Nano 2016, 10, 8517−8525

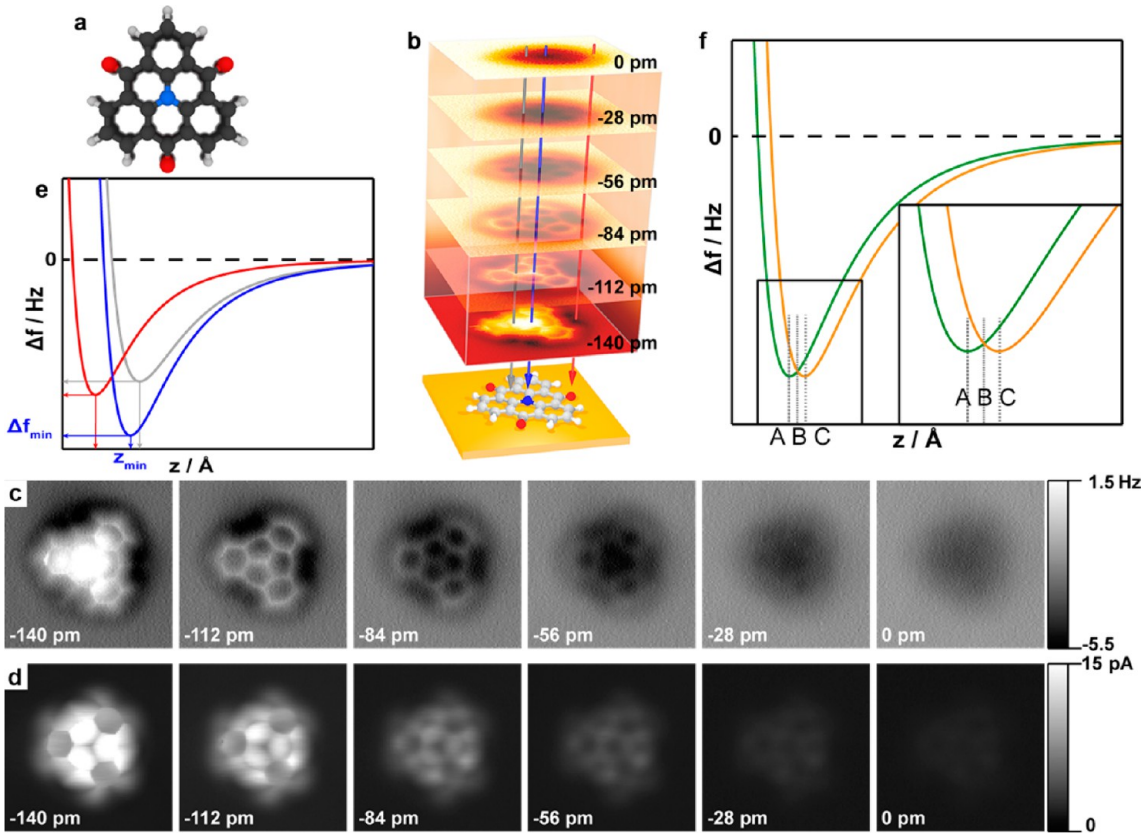

Figure 1. Acquisition and analysis of a 3D Δ*f* data cube over a model molecule. (a) Model of 1,5,9-trioxo-13-azatriangulene, which consists of carbon (black), nitrogen (blue), oxygen (red), and hydrogen (white) atoms. (b,c) Selection of constant height AFM images acquired with a CO-terminated tip. Indicated heights are with regard to an STM set point of 10 pA at 100 mV. (d) Simultaneously recorded current images. (e) Δ*f*(*z*) spectra can be extracted from the stack of constant height images shown in (b,c), indicated here by model curves (*i.e.*, the curves shown here do not represent experimental data). (f) Schematic curves with an offset in the vertical position of the minimum frequency shift, z_{min}, which may correspond to spectra acquired over different sites in a molecule.

and the chemical composition of the molecule, it may be possible to chemically recognize molecules on surfaces with AFM.

Here, we present a proof-of-concept study that demonstrates that maps of the minima of Δ*f*(*z*) curves, that is, maps of $z_{min}(x,y)$ and of $\Delta f_{min}(x,y)$, acquired over a molecule exhibit characteristic contrast. This contrast is reproduced in simulations based on molecular mechanics (MM) and DFT. We show that the vdW and Pauli interaction, together with the specific adsorption geometry of a given molecule on the surface, accounts for the observed contrast.

RESULTS AND DISCUSSION

We synthesized a planar three-fold rotationally symmetric model molecule, 1,5,9-trioxo-13-azatriangulene (TOAT) (Figure 1a), that contains H, C, N, and O atoms. The planarity eliminates effects due to vertical corrugation.[24] This model molecule was prepared using an established synthesis scheme.[25,26]

The 3D Δ*f* maps were acquired with CO-terminated tips by measuring stacks of 100 constant height AFM images with an interval of 7 pm over TOAT adsorbed on Cu(111). The image at the smallest tip−sample distance was taken at $\Delta z = -140$ pm with respect to an STM set point of $I = 10$ pA at $V = 0.1$ V. A selection from the experimental AFM images is shown in Figure 1b,c. In addition, Figure 1d shows the corresponding simultaneously recorded current images. The geometric structure of the molecule is clearly resolved. We extracted experimental Δ*f*(*z*) spectra over the molecule from the 3D data cube, as schematically illustrated in Figure 1b,e, from which we determined the $z_{min}(x,y)$ and $\Delta f_{min}(x,y)$ maps.

Before discussing these maps, we briefly discuss the advantage of acquiring and analyzing a 3D data grid over regular constant height images. The contrast in constant height AFM images sensitively depends on the height. However, also the *difference* in the contrast between sites can change as a function of tip−sample distance. For example, consider the two schematic Δ*f*(*z*) curves shown in Figure 1f. These could correspond to curves acquired over different sites in the molecule. Constant height images taken at tip−sample distances A and C will show an inverted contrast. Furthermore, if an image is taken at tip−sample distance B, the contrast at the two positions where the curves were acquired is identical. Since Δ*f*(*z*) curves—and their spatial variation—are not *a priori* known, it is impossible to know at which tip−sample distance to take an image. In contrast, $z_{min}(x,y)$ and $\Delta f_{min}(x,y)$ maps provide robust information.

The experimental work is complemented by a theoretical analysis. First, the adsorption geometry and charge distribution of TOAT on Cu(111) were calculated using total energy DFT simulations including vdW interactions. The relaxed geometry of the molecule on the surface is shown in Figure 2. Details can be found in the Supporting Information. The DFT results (charge distribution, adsorption geometry) were used as input for the MM-based simulation of the full 3D AFM data. The methods used in this second step have been described in detail elsewhere.[8,27−29] The mechanistic model includes the vdW and

DOI: 10.1021/acsnano.6b03644
ACS Nano 2016, 10, 8517−8525

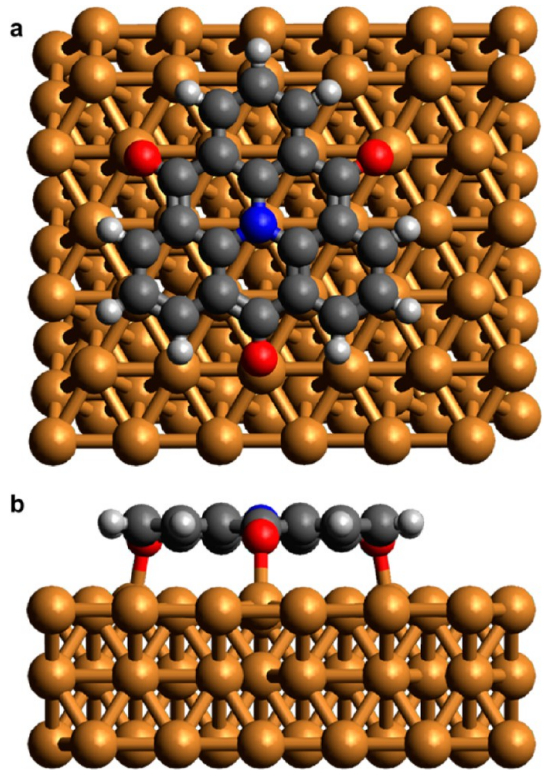

Figure 2. Fully relaxed atomic structure of TOAT on Cu(111) obtained from periodic DFT calculations including van der Waals interactions. (a) Top view. (b) Side view.

Pauli forces, as well as the electrostatic interactions between the tip and sample. The two main parameters in the mechanistic model are the lateral stiffness (k) of the probe particle–bulk tip junction and the effective charge (Q) of the probe particle. The parameters that provide the best agreement with experimental data were determined by comparing a stack of images simulated with different values of k and Q with experimental AFM images acquired at different heights above the molecule as described previously.[8] The as-determined values are $k = 0.24$ N/m and $Q = 0.0e^-$. These values are in fair agreement with previously reported values.[7,30,31] We note here that the effective charge of the CO will depend on how the molecule is adsorbed on the tip as well as on the chemical composition of the metallic tip apex to which it is bound. In addition, we added a long-range $\Delta f(z)$ component, estimated from experimental $\Delta f(z)$ spectra taken on the bare Cu(111) surface, to enable a direct comparison between the experimental and theoretical data.

The minima of the experimental and simulated $\Delta f(z)$ curves were found by fitting a parabola to points up to 1 Hz above the most negative Δf value. Over the lower lying Cu(111) substrate, the $\Delta f(z)$ spectra did not reach the minimum, which could therefore not be assigned. Contour plots of the as-determined values of experimental and simulated $z_{min}(x,y)$ and $\Delta f_{min}(x,y)$ maps are plotted in Figure 3a–d. Using the coordinates of the minimum of the curve to compare experimental data to simulated images enables us to review detailed information and small deviations visually. Extracting the location of the minimum from a $\Delta f(z)$ curve yields information about the effect and interplay of both repulsive and attractive forces. Alternatively, one can extract Lennard-Jones fit parameters from $\Delta f(z)$ spectra, but these are more prone to errors due to tip flexibility, especially at close distance. At distances where $z_{min}(x,y)$ and $\Delta f_{min}(x,y)$ are located, the lateral relaxation of the probe is still negligible.

The experimental and simulated $z_{min}(x,y)$ and $\Delta f_{min}(x,y)$ maps, shown in Figure 3, are overall in good agreement. Another set of maps, acquired with a different CO-terminated tip on a different molecule, is shown in the Supporting Information.

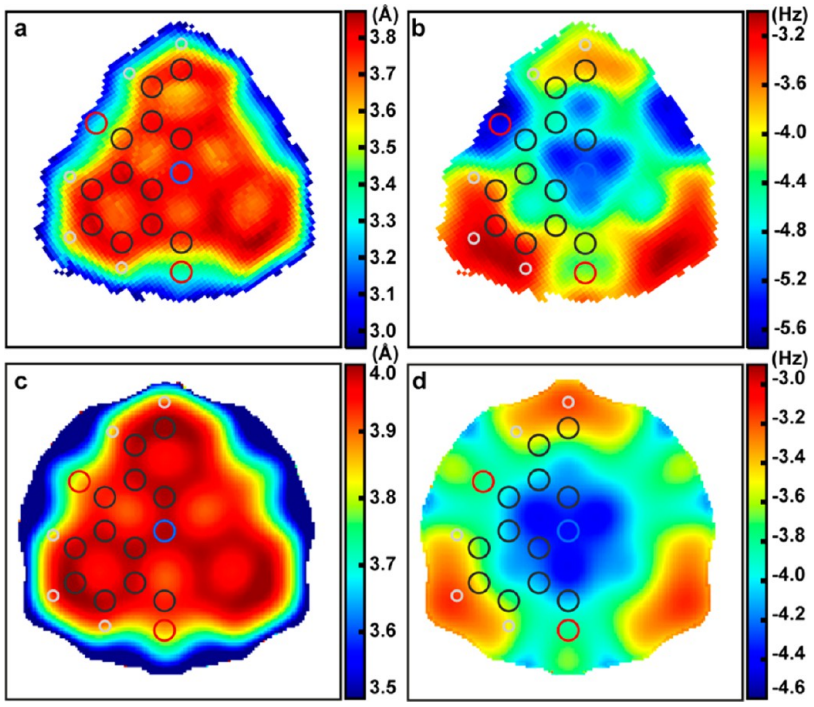

Figure 3. (a) Experimental $z_{min}(x,y)$ and (b) $\Delta f_{min}(x,y)$ maps, obtained with a CO-terminated tip. (c) Calculated $z_{min}(x,y)$ and (d) $\Delta f_{min}(x,y)$ maps. Theoretical $\Delta f_{min}(x,y)$ and $z_{min}(x,y)$ maps are calculated using a lateral stiffness $k = 0.24$ N/m and an effective charge on the CO tip of $Q = 0.0e^-$.

DOI: 10.1021/acsnano.6b03644
ACS Nano 2016, 10, 8517–8525

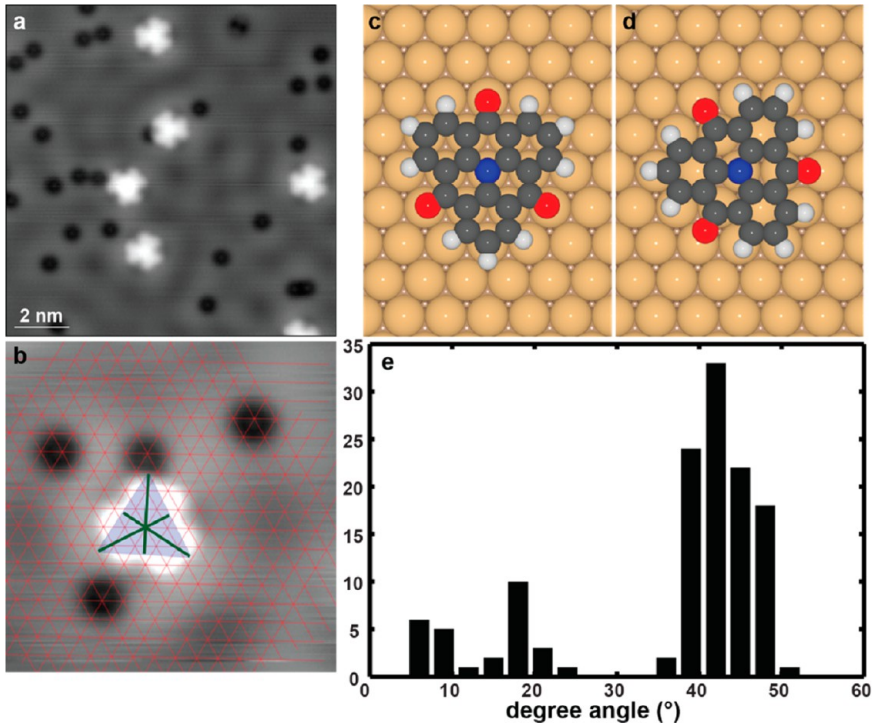

Figure 4. Study of adsorption orientation of TOAT on Cu(111). (a) STM image of six TOAT molecules and several CO molecules on Cu(111), acquired with a CO-terminated tip. (b) STM image of an adsorbed TOAT molecule and surrounding CO molecules, acquired with a CO-terminated tip. The dimensions of the overlaid grid correspond to the atomic configuration of the Cu(111) surface. (c,d) Schematic representation of a TOAT molecule adsorbed on Cu(111) between rows and along row orientations, respectively. (e) Histogram of relative angles of adsorbed TOAT molecules.

Above bonds/atoms, $z_{min}(x,y)$ is located at larger values of z compared to other positions (values of z refer to the height above the molecular plane). This is expected because, at these positions, repulsive interactions become more important at smaller tip−sample distances. Hence, the $z_{min}(x,y)$ maps resemble the structure of the molecule, including vertical corrugation within the molecule. The $\Delta f_{min}(x,y)$ maps feature more contrast. Above the benzene rings at the periphery, the minimum of the frequency shift is less negative (red) compared to the center of the molecule (blue). This is ascribed to the smaller vdW attraction at the edges. Note that the experimental maps do not extend as far outward from the center of the molecule as the simulated maps. Using an alternative approach, it should be possible to create $z_{min}(x,y)$ and $\Delta f_{min}(x,y)$ maps of the entire imaging area.[32] Our total energy calculations indicate a very shallow potential energy with respect to the vertical distortion of the oxygen atoms. The resulting uncertainty in the vertical position of the oxygen atoms will affect the contrast at these positions (see Supporting Information).

The contrast in the experimental $\Delta f_{min}(x,y)$ map has an imperfect three-fold symmetry. There can be multiple reasons for this. To investigate if this imperfect symmetry in the maps is due to a reduction of the symmetry induced by adsorption on the surface, we determined the adsorption configurations. We find that TOAT adsorbs on Cu(111) with two different orientations, rotated by 30°; see Figure 4. The adsorption configurations of both species was determined by using coevaporated CO molecules as markers (CO molecules are known to be adsorbed on top of Cu atoms[33]). An example is shown in Figure 4b. An analysis of multiple molecules consistently shows that in both configurations the N atom is adsorbed on top of a Cu atom. The two configurations correspond to molecules with their O atoms pointing between and along rows of Cu atoms (Figure 4c,d, respectively). Both of these adsorption geometries are three-fold symmetric. The imperfect symmetry in the experimental $\Delta f_{min}(x,y)$ map is therefore attributed to tip flexibility in conjunction with an asymmetric tip (on the mesoscopic scale).[19,29,34] This is further supported by the fact that maps acquired with a different CO-terminated tip on a different molecule exhibit a different symmetry (see Supporting Information).

To further investigate if the observed contrast in the $\Delta f_{min}(x,y)$ and $z_{min}(x,y)$ maps are molecule-specific, we take advantage of the good agreement of the simulated and experimental data. We calculated $\Delta f_{min}(x,y)$ and $z_{min}(x,y)$ maps with a CO tip for molecules with a different chemical composition but a similar structure. Specifically, we replaced the ketone groups by an ether (TOAT-ether) or a secondary amine (TOAT-amine), or we replaced the central N with a C (TOAT-C); see Figure 5a−c. In the latter case, one of the O atoms is changed into a hydroxyl group (OH) to maintain charge neutrality. Note that these molecules all have the same skeleton of conjugated carbon rings. However, each molecule has a distinct contrast in the $\Delta f_{min}(x,y)$ and $z_{min}(x,y)$ maps, and they are different from the maps of TOAT shown in Figure 3. Our DFT calculations revealed that these differences originate from different vdW interactions, as well as from changes in the atomic relaxation of the molecules on the surface.[26] This is in agreement with the observation of Schuler *et al.* that polycyclic aromatic hydrocarbons that have a different functional group have a different adsorption height.[35]

The $\Delta f_{min}(x,y)$ maps also exhibit clear differences, especially at the periphery, where the different functional groups are located. In particular, there is a shift in location and depth of the well, indicated by green arrows in Figure 5g−i. The calculated $\Delta f_{min}(x,y)$ of TOAT-C (Figure 4f) contains an asymmetry caused by the OH group on the periphery. From this

DOI: 10.1021/acsnano.6b03644
ACS Nano 2016, 10, 8517−8525

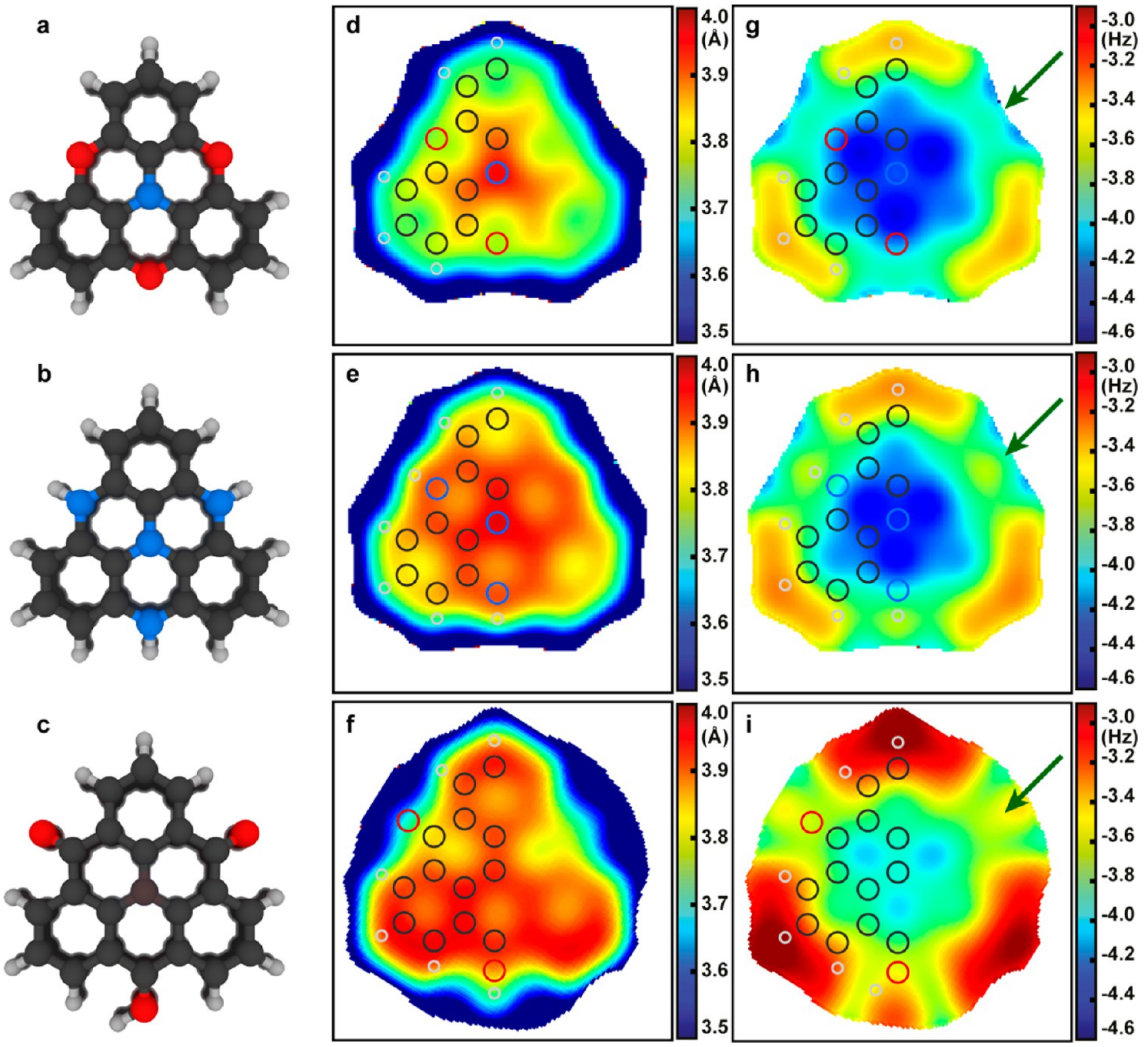

Figure 5. Schematic representations of theoretically investigated molecules, where ketone groups in TOAT are replaced by (a) an ether (TOAT-ether), (b) a secondary amine (TOAT-amine), (c) the central N with a C (TOAT-C). Calculated $z_{min}(x,y)$ maps for (d) TOAT-ether, (e) TOAT-amine, (f) TOAT-C. Calculated $\Delta f_{min}(x,y)$ maps for (g) TOAT-ether, (h) TOAT-amine, (i) TOAT-C. Theoretical $\Delta f_{min}(x,y)$ and $z_{min}(x,y)$ are calculated with a lateral stiffness of k = 0.24 N/m and an effective charge on the CO tip of $Q = 0.0e^-$.

comparison, it is evident that $\Delta f_{min}(x,y)$ and $z_{min}(x,y)$ maps can be used to discriminate between molecules.

We now turn our attention to the origin of the characteristic contrast. Since the simulations without including electrostatic forces (the effective charge Q on the tip is zero) can reproduce the experimental observations very well, electrostatic forces cannot be responsible for the characteristic contrast. Hence, the vdW and Pauli interaction, together with the specific adsorption geometry of a given molecule on the surface, must therefore account for the contrast. At the distance of most negative frequency shift, that is, at the z corresponding to Δf_{min}, the vdW component is dominant.

Considering that discussed above, the contrast in the $z_{min}(x,y)$ and $\Delta f_{min}(x,y)$ maps may be blurred for probes with a large atomic radius (*e.g.*, Xe) and/or a significant charge. A larger probe radius leads to increased interactions with neighboring atoms, resulting in an averaging effect. Charged tips may not be suitable since the charge distribution in molecules typically varies rather slowly, and regions of increased charge density are not necessarily localized on atoms. We note here that the large majority of the molecules have a nonhomogeneous charge distribution.

To support this interpretation of the contrast mechanism, we repeated the experiment and simulations with a positively charged Xe-terminated tip (parameters: $Q = +0.3e^-$ and k = 0.24 N/m).[8] A selection from the constant height AFM images and the corresponding I images is shown in Figure 6.

Figure 7 shows the experimental and theoretical $z_{min}(x,y)$ and $\Delta f_{min}(x,y)$ maps extracted from the 3D data. The simulated and experimental maps show, just like for the CO tip, very good agreement. However, in contrast to the maps acquired with CO tips, both $\Delta f_{min}(x,y)$ and $z_{min}(x,y)$ maps acquired with Xe-terminated tips show very little features. Our theoretical analysis shows that the loss of resolution is driven by both (i) the large atomic radius of Xe and (ii) the pronounced electrostatic interaction between the charged probe and the molecule. Because of these two reasons, Xe-terminated tips are less suitable for chemical recognition of molecules.

The C and N atoms in the center of the molecule have a similar chemical and geometric environment. In addition, the gradient of the underlying vdW background is small in the interior of the molecule. Furthermore, their central location is important to minimize the influence of tip relaxations (*i.e.*, bending of the CO).[24] Hence, for this molecule, $\Delta f(z)$ spectra acquired above C

DOI: 10.1021/acsnano.6b03644
ACS Nano 2016, 10, 8517−8525

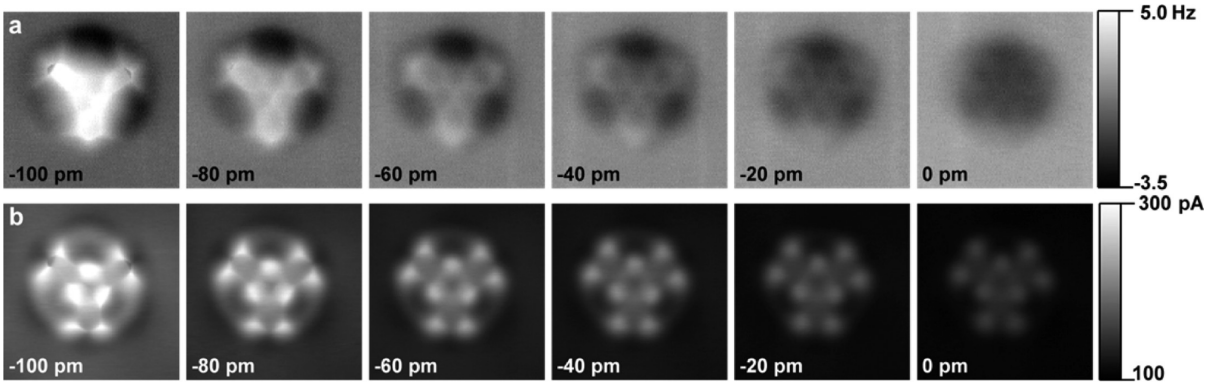

Figure 6. Selection of images from 3D mapping, recorded with a Xe-terminated tip. (a) Selection of constant height AFM images. (b) Simultaneously recorded *I* images. Indicated heights are with regard to STM set point of 500 pA at 200 mV.

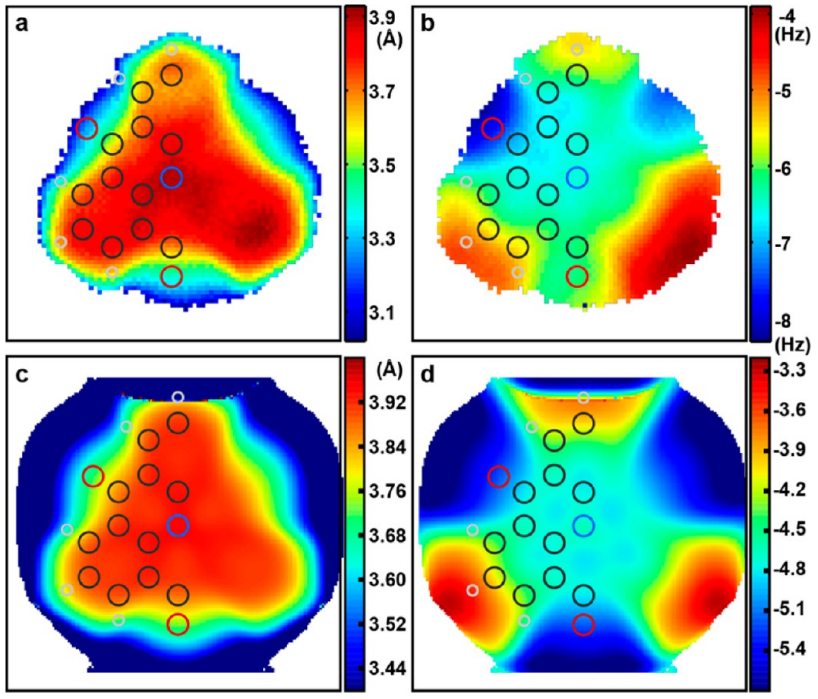

Figure 7. (a) Experimental $z_{min}(x,y)$ and (b) $\Delta f_{min}(x,y)$ maps, obtained with a Xe-terminated tip. (c) Calculated $z_{min}(x,y)$ and (d) $\Delta f_{min}(x,y)$ maps. Theoretical $\Delta f_{min}(x,y)$ and $z_{min}(x,y)$ are calculated with a lateral stiffness of k = 0.24 N/m and an effective charge on the Xe tip of $Q = +0.3e^{-}$.

and N in the center can be compared on (almost) equal footing. Figure 8a shows $\Delta f(z)$ spectra extracted from the same 3D data set as was used to compile the $\Delta f_{min}(x,y)$ and $z_{min}(x,y)$ maps in Figure 3. The (x,y) positions approximately correspond to the location of a N (blue) and three equivalent C (black) atoms, respectively (see inset). The coordinates of the minimum are distinctly different for the different atoms: the well above the central N atom (blue curve) is deeper than that above a C atom (black curve). The value of z_{min} for both atoms is the same within experimental error, indicating that they have the same adsorption height to within a few picometers. This is in good agreement with the DFT calculations. The differences between the chemically and geometrically equivalent C atoms are much smaller than the difference between C and N. The calculated $\Delta f(z)$ spectra over these atoms are shown in Figure 8b and reproduce the experimentally observed trend.

To examine the influence of the adsorption site on the $\Delta f(z)$ curves, spectra were simultaneously acquired above molecules in both configurations. Figure 8c shows a constant height AFM image of two molecules with different adsorption configuration. As shown in Figure 8d, spectra acquired over equivalent positions over the two molecules overlap within experimental error. Note that the trend is the same as observed in the spectra extracted from the 3D data cube: Δf_{min} is significantly more negative for N than for the neighboring C atoms. This trend should hold for all tertiary amines (N atom coordinated to three C atoms) and C atoms that have a similar geometric and chemical environment (including adsorption height and interaction with the surface). The absolute values differ between experiments due to different macroscopic atomic tip clusters, resulting in different vdW contributions.

CONCLUSION

In summary, we showed that maps of $z_{min}(x,y)$ and $\Delta f_{min}(x,y)$ acquired with CO-terminated tips have distinct characteristics that can differentiate between structurally similar molecules on surfaces. The characteristic contrast in these maps originates from the vdW interactions between tip and molecule, as well as

DOI: 10.1021/acsnano.6b03644
ACS Nano 2016, 10, 8517–8525

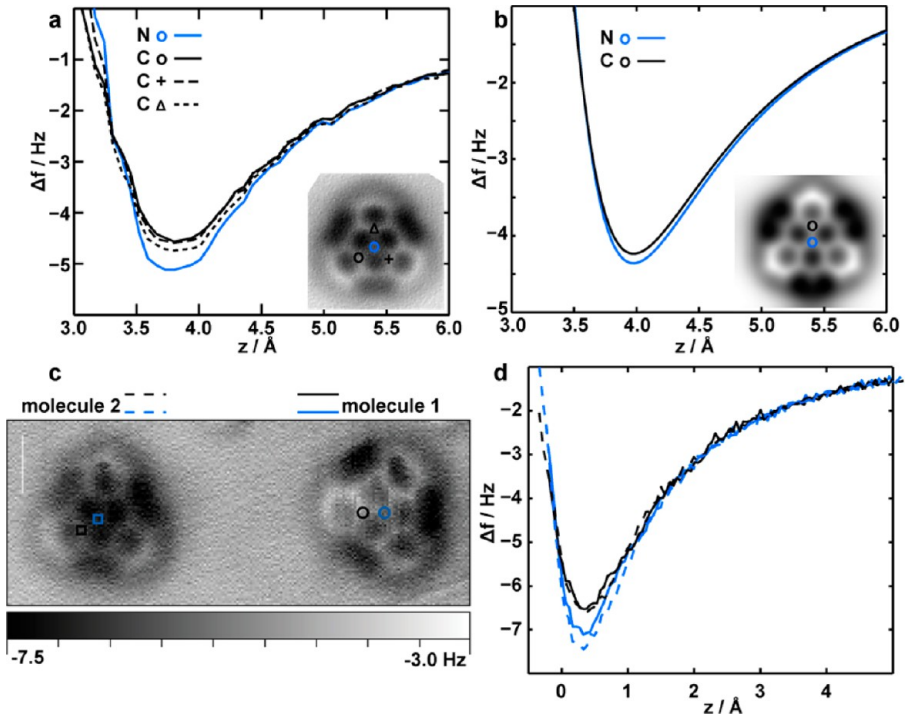

Figure 8. Additional $\Delta f(z)$ spectra over TOAT molecules with CO-terminated tips. (a) $\Delta f(z)$ spectra extracted from the 3D data grid over selected positions on TOAT, as indicated in the inset. The $\Delta f(z)$ spectra are the average of nine curves of a 3 × 3 pixel area; *i.e.*, each spectrum is the average of the spectra of the selected pixel and the pixels touching the selected one. (b) Calculated $\Delta f(z)$ spectra extracted over selected positions on TOAT, as indicated in the inset. (c) Constant height AFM image of two molecules in different orientation, at −130 pm with regard to the STM set point of 10 pA at 100 mV. Molecule 1 and molecule 2 lie with their peripheral O atoms between and along atomic rows, respectively. (d) Individual $\Delta f(z)$ spectra acquired above the same atoms as in (a) and (b) over the two molecules in (c), where z = 0 Å corresponds to the imaging height of (c). The z alues of molecule 1 are corrected for z-drift using the following procedure. Immediately prior to the AFM experiment, an $I(z)$ curve was acquired (with the same oscillation amplitude and bias). These data were used to convert the observed changes in the tunnel current during the constant height experiment to a change in tip−sample distance. The z-drift between acquisition of the two $\Delta f(z)$ spectra was 0.35 Å.

from the adsorption geometry of the molecule on the surface. Since the adsorption height (and its variations within a molecule) strongly depend on the interaction between the molecule and the substrate, the $z_{min}(x,y)$ and $\Delta f_{min}(x,y)$ maps of a particular molecule should be substrate-dependent. The trends in z position and the depth of the minimum are the same for all CO-terminated tips, while the absolute values differ from tip to tip. Tips employing larger atoms and/or tips with a significant charge (like Xe) are less suitable for chemical recognition of molecules.

The force resolution required to apply the procedure outlined here is on the order of 1 pN/100 mHz (for a typical qPlus sensor). This criterion is typically fulfilled in cases where submolecular resolution imaging of molecules has been reported.

METHODS

Synthesis of 1,5,9-Trioxo-13-azatriangulene. The synthesis reported herein is based on literature procedures.[25] For the sake of completeness and reproducibility, we describe the procedure and our observations. The first step is the systhesis of tris(*ortho*-methylbenzoate)-amine (TOMBA). TOMBA was synthesized by refluxing a solution in diphenyl ether of 1:3:2 parts of 2-aminobenzoic acid methyl ester, 2-iodobenzoic acid methyl ester, and potassium carbonate, respectively, in the presence of copper and copper(I) iodide, for 16 h at 210 °C under nitrogen atmosphere. After purification, the yield was 76%. The purified TOMBA was subsequently used to synthesize TOAT. A solution of TOMBA in 98% H_2SO_4 was heated to 105 °C and kept at that temperature for 24 h. After purification, the yield was 7.2% (46.9 mg). Further details of the synthesis, purification, and spectra can be found in the Supporting Information.[26]

STM and AFM Measurements. We used an Omicron Nanotechnology LT STM/AFM with a commercially available qPlus sensor, operating at approximately 4.6 K in ultrahigh vacuum with an average pressure of 5 × 10^{-10} mbar. A Cu(111) crystal surface was cleaned with several sputter and anneal cycles before being inserted into the microscope head. The TOAT molecules were thermally evaporated onto the cold surface using a Knudsen cell-type evaporator. For STM imaging, the bias voltage was applied to the sample. The baked qPlus sensor (3 h at 120 °C) had a quality factor of $Q \approx 30\,000$, a resonance frequency of f_0 = 25 634 Hz, and a peak-to-peak oscillation amplitude of <2 Å. After the tip approached the surface, it often needed some preparation to sharpen the apex and ensure stability. This was accomplished with controlled crashes into the copper surface and bias pulses until the STM resolution was satisfactory. The tip apex was functionalized with a single CO molecule following the standard method.[36] After an appropriate TOAT molecule was located on the surface, the tip was left in tunneling contact (I = 10 pA at V = 0.1 V) and allowed to relax for 12 h to prevent drift and creep. After this time, there was no detectable x- or y-drift. To compensate for z-drift, the STM feedback was turned on for 2 s after each constant height AFM image and then turned off again before adjusting the height for the next image. No data analysis procedures such as those described in ref 37 were therefore necessary. The AFM was operated in constant height mode, and AFM images show the frequency shift (Δf) with respect to the resonance frequency.

Specific acquisition parameters for the maps presented in this article are as follows. The stack resulting in the maps of Figure 4 consisted of 100 images, from −140 pm to +553 pm with regard to an STM set point of 10 pA at 100 mV, in steps of 7 pm. The spectra in Figure 8a were extracted from this stack. The stack resulting in the maps of Figure 7 had 35 images, from −100 pm to +75 pm with regard to an STM set point of 500 pA at 200 mV.

DOI: 10.1021/acsnano.6b03644
ACS Nano 2016, 10, 8517−8525

Theoretical Modeling. Simulations were performed using MM calculations using geometries and charge distributions as determined from DFT calculations.[26]

ASSOCIATED CONTENT

Supporting Information

The Supporting Information is available free of charge on the ACS Publications website at DOI: 10.1021/acsnano.6b03644.

Synthesis of 1,5,9-trioxo-13-azatriangulene, brief description of DFT modeling, brief description of the mechanical probe particle AFM model (PDF)

AUTHOR INFORMATION

Corresponding Author

*E-mail: i.swart@uu.nl.

Notes

The authors declare no competing financial interest.

ACKNOWLEDGMENTS

We thank Daniël Vanmaekelbergh for valuable discussions. Financial support from the Nederlandse Organisatie voor Wetenschappelijk Onderzoek (ECHO-Stip Grant No. 717.013.003), the GAČR (Project No. 14-16963J), and the BioSolar Cells Program of the Dutch Ministry of Economic Affairs is gratefully acknowledged.

REFERENCES

(1) Repp, J.; Meyer, G.; Stojković, S. M.; Gourdon, A.; Joachim, C. Molecules on Insulating Films: Scanning-Tunneling Microscopy Imaging of Individual Molecular Orbitals. *Phys. Rev. Lett.* **2005**, *94*, 26803.

(2) Gross, L.; Mohn, F.; Moll, N.; Liljeroth, P.; Meyer, G. The Chemical Structure of a Molecule Resolved by Atomic Force Microscopy. *Science* **2009**, *325*, 1110−1114.

(3) Weiss, C.; Wagner, C.; Tautz, F. S.; Temirov, R. Direct Imaging of Intermolecular Bonds in Scanning Tunneling Microscopy. *J. Am. Chem. Soc.* **2010**, *132*, 11864.

(4) Chiang, C. -l.; Xu, C.; Han, Z.; Ho, W. Real-Space Imaging of Molecular Structure and Chemical Bonding by Single-Molecule Inelastic Tunneling Probe. *Science* **2014**, *344*, 885−888.

(5) Mohn, F.; Gross, L.; Moll, N.; Meyer, G. Imaging the Charge Distribution within a Single Molecule. *Nat. Nanotechnol.* **2012**, *7*, 227−231.

(6) Gross, L.; Moll, N.; Mohn, F.; Curioni, A.; Meyer, G.; Hanke, F.; Persson, M. High-Resolution Molecular Orbital Imaging Using a P-Wave STM Tip. *Phys. Rev. Lett.* **2011**, *107*, 86101.

(7) Gross, L.; Mohn, F.; Moll, N.; Schuler, B.; Criado, A.; Guitian, E.; Pena, D.; Gourdon, A.; Meyer, G.; Guitián, E.; et al. Bond-Order Discrimination by Atomic Force Microscopy. *Science* **2012**, *337*, 1326−1329.

(8) Hapala, P.; Svec, M.; van der Heijden, N. J.; van der Lit, J.; Stetsovych, O.; Ondrácek, M.; Mutombo, P.; Swart, I.; Jelinek, P. Mapping the Electrostatic Force Field of Single Molecules from High-Resolution Scanning Probe Images. *Nat. Commun.* **2016**, *7*, 11560.

(9) Stipe, B. C. Single-Molecule Vibrational Spectroscopy and Microscopy. *Science* **1998**, *280*, 1732−1735.

(10) Schmid, M.; Stadler, H.; Varga, P. Direct Observation of Surface Chemical Order by Scanning Tunneling Microscopy. *Phys. Rev. Lett.* **1993**, *70*, 1441−1444.

(11) Varga, P.; Schmid, M. Chemical Discrimination on Atomic Level by STM. *Appl. Surf. Sci.* **1999**, *141*, 287−293.

(12) Jiang, J.; Kula, M.; Luo, Y. Molecular Modeling of Inelastic Electron Transport in Molecular Junctions. *J. Phys.: Condens. Matter* **2008**, *20*, 374110.

(13) Lantz, M. A.; Hug, H. J.; Hoffmann, R.; van Schendel, P. J. A.; Kappenberger, P.; Martin, S.; Baratoff, A.; Güntherodt, H. J. Quantitative Measurement of Short-Range Chemical Bonding Forces. *Science* **2001**, *291*, 2580−2583.

(14) Sugimoto, Y.; Pou, P.; Abe, M.; Jelinek, P.; Perez, R.; Morita, S.; Custance, O. Chemical Identification of Individual Surface Atoms by Atomic Force Microscopy. *Nature* **2007**, *446*, 64−67.

(15) Setvín, M.; Mutombo, P.; Ondráček, M.; Majzik, Z.; Švec, M.; Cháb, V.; Ošťádal, I.; Sobotík, P.; Jelínek, P. Chemical Identification of Single Atoms in Heterogeneous III−IV Chains on Si(100) Surface by Means of Nc-AFM and DFT Calculations. *ACS Nano* **2012**, *6*, 6969−6976.

(16) Teobaldi, G.; Lammle, K.; Trevethan, T.; Watkins, M.; Schwarz, A.; Wiesendanger, R.; Shluger, A. L. Chemical Resolution at Ionic Crystal Surfaces Using Dynamic Atomic Force Microscopy with Metallic Tips. *Phys. Rev. Lett.* **2011**, *106*, 216102.

(17) Welker, J.; Weymouth, A. J.; Giessibl, F. J. The Influence of Chemical Bonding Configuration on Atomic Identification by Force Spectroscopy. *ACS Nano* **2013**, *7*, 7377−7382.

(18) Baykara, M. Z.; Todorović, M.; Mönig, H.; Schwendemann, T. C.; Ünverdi, Ö.; Rodrigo, L.; Altman, E. I.; Pérez, R.; Schwarz, U. D. Atom-Specific Forces and Defect Identification on Surface-Oxidized Cu(100) with Combined 3D-AFM and STM Measurements. *Phys. Rev. B: Condens. Matter Mater. Phys.* **2013**, *87*, 155414.

(19) Hölscher, H.; Langkat, S. M.; Schwarz, a.; Wiesendanger, R. Measurement of Three-Dimensional Force Fields with Atomic Resolution Using Dynamic Force Spectroscopy. *Appl. Phys. Lett.* **2002**, *81*, 4428−4430.

(20) Gross, L.; Mohn, F.; Moll, N.; Meyer, G.; Ebel, R.; Abdel-Mageed, W. M.; Jaspars, M. Organic Structure Determination Using Atomic-Resolution Scanning Probe Microscopy. *Nat. Chem.* **2010**, *2*, 821−825.

(21) Schuler, B.; Meyer, G.; Peña, D.; Mullins, O. C.; Gross, L. Unraveling the Molecular Structures of Asphaltenes by Atomic Force Microscopy. *J. Am. Chem. Soc.* **2015**, *137*, 9870−9876.

(22) Kawai, S.; Saito, S.; Osumi, S.; Yamaguchi, S.; Foster, A. S.; Spijker, P.; Meyer, E. Atomically Controlled Substitutional Boron-Doping of Graphene Nanoribbons. *Nat. Commun.* **2015**, *6*, 8098.

(23) Moll, N.; Gross, L.; Mohn, F.; Curioni, A.; Meyer, G. The Mechanisms Underlying the Enhanced Resolution of Atomic Force Microscopy with Functionalized Tips. *New J. Phys.* **2010**, *12*, 125020.

(24) Boneschanscher, M. P.; Hämäläinen, S. K.; Liljeroth, P.; Swart, I. Sample Corrugation Affects the Apparent Bond Lengths in Atomic Force Microscopy. *ACS Nano* **2014**, *8*, 3006−3014.

(25) Hellwinkel, D.; Melan, M. Heteropolycyclen Vom Triangulen-Typ, I. 8.12-Dihydro-4H-benzo[1.9]chinolizino[3.4.5.6.7-Defg]acridin-Trion-(4.8.12) Und 5.9-Dihydro-chino[3.2.1-De]acridin-Dion-(5.9). *Chem. Ber.* **1971**, *104*, 1001−1016.

(26) See Supporting Information.

(27) Hämäläinen, S. K.; van der Heijden, N.; van der Lit, J.; den Hartog, S.; Liljeroth, P.; Swart, I. Intermolecular Contrast in Atomic Force Microscopy Images without Intermolecular Bonds. *Phys. Rev. Lett.* **2014**, *113*, 186102.

(28) Hapala, P.; Temirov, R.; Tautz, F. S.; Jelinek, P. Origin of High-Resolution IETS-STM Images of Organic Molecules with Functionalized Tips. *Phys. Rev. Lett.* **2014**, *113*, 226101.

(29) Hapala, P.; Kichin, G.; Wagner, C.; Tautz, F. S.; Temirov, R.; Jelínek, P. Mechanism of High-Resolution STM/AFM Imaging with Functionalized Tips. *Phys. Rev. B: Condens. Matter Mater. Phys.* **2014**, *90*, 085421.

(30) Weymouth, A. J.; Hofmann, T.; Giessibl, F. J. Quantifying Molecular Stiffness and Interaction with Lateral Force Microscopy. *Science* **2014**, *343*, 1120−1122.

(31) van der Lit, J.; Di Cicco, F.; Hapala, P.; Jelinek, P.; Swart, I. Submolecular Resolution Imaging of Molecules by Atomic Force Microscopy: The Influence of the Electrostatic Force. *Phys. Rev. Lett.* **2016**, *116*, 096102.

(32) Mohn, F.; Gross, L.; Meyer, G. Measuring the Short-Range Force Field above a Single Molecule with Atomic Resolution. *Appl. Phys. Lett.* **2011**, *99*, 053106.

DOI: 10.1021/acsnano.6b03644
ACS Nano 2016, 10, 8517−8525

(33) Ishi, S.; Ohno, Y.; Viswanathan, B. An Overview on the Electronic and Vibrational Properties of Adsorbed CO. *Surf. Sci.* **1985**, *161*, 349–372.
(34) Gao, D. Z.; Grenz, J.; Watkins, M. B.; Federici Canova, F.; Schwarz, A.; Wiesendanger, R.; Shluger, A. L. Using Metallic Noncontact Atomic Force Microscope Tips for Imaging Insulators and Polar Molecules: Tip Characterization and Imaging Mechanisms. *ACS Nano* **2014**, *8*, 5339–5351.
(35) Schuler, B.; Liu, W.; Tkatchenko, A.; Moll, N.; Meyer, G.; Mistry, A.; Fox, D.; Gross, L. Adsorption Geometry Determination of Single Molecules by Atomic Force Microscopy. *Phys. Rev. Lett.* **2013**, *111*, 106103.
(36) Bartels, L.; Meyer, G.; Rieder, K. H. Controlled Vertical Manipulation of Single CO Molecules with the Scanning Tunneling Microscope: A Route to Chemical Contrast. *Appl. Phys. Lett.* **1997**, *71*, 213–215.
(37) Albers, B. J.; Schwendemann, T. C.; Baykara, M. Z.; Pilet, N.; Liebmann, M.; Altman, E. I.; Schwarz, U. D. Data Acquisition and Analysis Procedures for High-Resolution Atomic Force Microscopy in Three Dimensions. *Nanotechnology* **2009**, *20*, 264002.

DOI: 10.1021/acsnano.6b03644
ACS Nano 2016, 10, 8517–8525